# Small Fullerenes with BN Belts: A Density Functional Theory Investigation

**Fengyi Liu, Lingpeng Meng,* and Shijun Zheng**

*Open Laboratory of Computational Quantum Chemistry, Hebei Normal University, Shijiazhuang 050016, P. R. China*

*Received: December 16, 2005; In Final Form: February 7, 2006*

Density functional calculations have been carried out on a series of BCN hybrid fullerenes with certain substitution patterns in comparison with their parent compounds $C_n$ ($n$ = 30, 32, 36, 38, 40, 44, 48, 50, 52). The substitutional structures, energy gaps between the highest occupied molecular orbital and the lowest unoccupied molecular orbital, ionization potentials, electron affinities, as well as molecular electrostatic potentials have been systematically investigated. The following important points of BCN hybrid fullerenes are stressed: The present studied fullerenes, comprising tubular "belt" and polar "cap", could be divided into three types of structure; each has different indexes of tubular structure and terminal caps. The properties of BCN hybrid fullerenes depend on the type of "tubular belt + polar cap" structures, especially, the HOMO and LUMO characters and MEPs of BCN fullerene are strongly governed by their structure types.

## Introduction

Since the discovery of $C_{60}$ in 1985[1] and carbon nanotubes (C-NTs) in 1991,[2] these fantastic allotropes of carbon have stimulated intense experimental and theoretical studies[3−12] because both have remarkable physical, chemical, and electronic properties and might have potential applications as superconductors, photoelectronic devices, semiconductors, nanometer electronics, etc.[13−15]

At the same time, some limitations were inevitably encountered further studies and applications of fullerenes and C-NTs due to their inherent vices. For instance, most fullerenes smaller than $C_{60}$ can only be observed and characterized in the gas phase, whereas the efforts made for bulk synthesis have proven to be mostly fruitless because of their high labilities.[16] In the meantime it has also been demonstrated both theoretically and experimentally that substitutional doping of heteroatoms (including B, N, BN, etc.) into fullerenes would produce significant changes in the charge distributions, electronic structures, and energy gaps between the lowest unoccupied molecular orbital (LUMO) and the highest occupied molecular orbital (HOMO) of the parent cages.[17−19] Thus, though the pure carbon fullerenes might be synthetically approachable, small fullerenes can definitely be stabilized by substitutional functionalization.[16] The same fate was found in the applications of C-NTs as nanoelectronic devices (such as field-effect nanotransistors, etc.), i.e., instead of the index ($n$, $m$) of the tube, the electronic properties of a C-NT are mainly governed by the tube chirality. Until now, no method was found to reliably separate C-NTs with different chiralities.[20] Once again, BN substitutional doping was tested to be a key to resolve this problem. Unlike their carbon analogues, boron nitride nanotubes (BN-NTs) have a uniform electronic band gap independent of the diameter and chirality of tube.[21,22] Introducing BN impurities into C-NTs is expected to provide the possibility of new types of materials with tunable electronic properties. As a result, BN doping can enhance the chemical stabilities of fullerene and C-NTs and open new pathways to the synthesis of new compounds.

* To whom correspondence should be addressed. Fax: 86-311-86269217. E-mail: menglp@mail.hebtu.edu.cn.

The selection of BN as dopants in fullerenes and C-NTs is natural. BN is isoelectronic with $C_2$, and boron nitride exists in both hexagonal (*h*-BN) and cubic phases (*c*-BN) that are structurally similar to the commonly known graphite and diamond phases of carbon. Furthermore, the B═N bond distances are 145 pm in boron nitride, which is within the range of C−C bond distances of the fullerene and C-NTs (140 and 146 pm).[21] Thus, doping of BN will not significantly alter the structure of the parent compounds, so the doping procedures are expected to be easily carried out. The BN doping system where CC moieties of carbon compounds were partially substituted by boron nitride units, which is known as the BCN system, is expected to be a hybrid of the parent compound and BN materials with desirable properties such as extreme hardness, low dielectric constant, chemical inertness, and high-temperature resistance to oxidation. Out of the BCN fullerenes studied so far, overwhelming attention has been paid to establish optimal BN substitution patterns in fullerene-like cage structures.[23−27] Kar et al. suggested several rules in their previous investigations including "hexagon-hexagon junction", "hexagon filling", and "continuity". Along these rules, a new series of hybrid BCN fullerenes in certain substitution patterns and with high stabilities could be proposed and attracted our research interest.

As shown in Chart 1, the new BCN hybrid fullerenes have BN hexagon−hexagon (h−h) junction "belts" along the equator and unsubstituted carbon moieties on each side. The parallelism between small stable fullerenes and carbon nanotubes (C-NTs) has been well established, e.g., $C_{60}$, $C_{36}$, and $C_{20}$ were considered to be associated with the smallest C-NTs with diameters of 0.7,[28] 0.5,[29] and 0.4[30] nm, respectively. This consistency is expected to be valid for the BCN system also. The structure of BCN fullerenes illustrated in Chart 1 could be regarded as a combination of basic BN nanotubes (BN-NTs) and carbon caps, e.g., $C_{20}B_{20}N_{20}$ suggested by Kar et al.[25] could be considered as arm chair (*5*, *5*) BN-NTs and five carbons pairs intact on each side of the BN tube, while $C_{10}B_{10}N_{10}$ (BN-substituted analog of $C_{30}$) includes a zigzag (*5*, *0*) BN-NT ended with two carbon hexagonal caps. In another words, they are carbon fullerenes with BN belts or BN-NTs with carbon endings.

10.1021/jp057350y CCC: $33.50 
Published on Web 03/09/2006

**CHART 1: CBN Fullerene vs BN Nanotube with Carbon Caps**

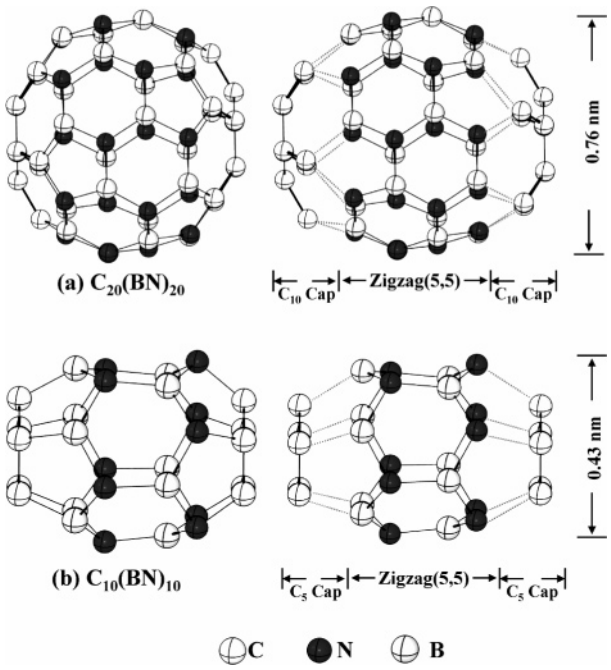


Recently, Xu et al.[27] also reported a similar equatorial BN belt compound $C_{20}(BN)_{15}$ as thermodynamically and chemically the most stable one among the isomers of $C_{50-2x}(BN)_x$, and they further proposed this isomer to be a potential CBN ball material. Therefore, these novel hybrid structures are not merely fullerenes with colorful belts in visualization tools but also expected to be intermediate compounds between fullerenes and BN-NTs with unique properties differing from both fullerene and the open-end BN-NTs. Though the carbon fullerenes and C-NTs as well as their BCN counterparts are well developed, to our knowledge, structures with an equatorial BN belt proposed here are still unknown.

In the present investigation the full equatorial hexagonal-substituted BCN system as well as their parent fullerenes $C_n$ ($n < 60$) with hexagon−hexagon junction belts including $C_{30}$ ($D_{2v}$), $C_{32}$ ($D_{3d}$), $C_{36}$ ($D_{6h}$), $C_{38}$ ($C_{3h}$), $C_{40}$ ($C_{2h}$), $C_{44}$ ($D_{3d}$), $C_{48}$ ($D_{6d}$), $C_{50}$ ($C_{2v}$), and $C_{52}$ ($C_{3v}$) were considered. We are interested in revealing the geometrical and electronic structures of BCN fullerenes, comparing them with their well-known carbon analogues. The results of this work might lead to nanoparticles with unusual electronic properties as promising candidates for electronic devices.

## Method of Calculations

$C_n$ ($n < 60$) has many conventional cage isomers, e.g., $C_{30}$ has three fullerene isomers, isomers of $C_{36}$ up to 15, and $C_{40}$ and $C_{50}$ have as many as 40 and 271 fullerene-like isomers, respectively (more details about fullerene isomers can be found in refs 16 and 31). Thus, neither was excessive effort made in systematic structural searching nor was attention paid to the energy-favorable isomers; the isomers selected here are the ones with hexagon−hexagon junction belts and the highest degree of principal axis, which directly associates with the simplest topological structures of C-NTs (zigzag or armchair type). For instance, among the 40 fullerene isomers of $C_{40}$, two have a $D_5$ principal axis, one is oblate and the other is an elongate cage containing a zigzag (*5, 0*) C-NT-like side wall (structures are not shown). Hence, the latter $D_{5d}$ isomer was selected as the starting point of the 40-member BCN fullerene. The same strategy was employed in choosing other C-NTs-contained isomers of fullerenes.

Because neither theoretical calculations nor experimental results on this series of BCN hybrid system have been reported so far, initially full geometry optimizations of all parent compounds $C_n$ ($n = 30, 32, 36, 38, 40, 44, 48, 50, 52$) as well as their BN-substituted analogues were performed using the B3LYP[32,33] function in the absence of symmetry constraints. The molecules were optimized at the split-valence double-$\xi$ basis function 3-21G* level which uses one polarization function for each atom.

Besides their structural information, we intend to describe the energy gaps between the LUMO and HOMO, charge distributions, electron affinities (EA), and ionization potential (IP) as well as the molecular electrostatic potential (MEP)[34] of the BCN hybrid system. These properties are known to be closely related to the band gap, kinetic stability, and aromatic character in conjugated systems. Hence, single-point energy calculations were carried out at B3LYP/6-31G* level based on the B3LYP/3-21G*-optimized geometries; then the LUMO and LUMO energies and corresponding orbital characters were obtained.

The electron affinity (EA) and ionization potential (IP) of carbon and hybrid fullerenes were obtained using a subtraction strategy, instead of Koopmann's theorem, which was originally based on Hartree−Fock (HF) orbitals other than Kohn−Sham orbitals. The vertical EA refers to the energy difference between the optimized neutral state and the anionic state in the geometry of the neutral state, whereas the vertical IP corresponds to the energy difference between the cationic state in the geometry of the neutral state and the optimized neutral state.

Finally, The MEP has been employed as an informative tool to describe the molecular reactivity and intermolecular interactions. In general, negative electrostatic potentials are usually associated with the lone pairs of the more electronegative atoms and unsaturated aromatic as well as strained carbon−carbon bonds; hence, they give valuable information about the $\pi$-electron delocalization and aromatic character in conjugated systems. The electrostatic potential in the current work is generated based on the total molecular charge distribution during B3LYP/6-31G* SCF calculations.

All calculations were performed with the Gaussian 98 program.[35]

## Results and Discussion

The optimized geometries of the $C_n$ ($n = 30, 32, 36, 38, 40, 44, 48, 50, 52$) fullerenes (*S1*−*S9*) and their BCN counterparts (*1*−*9*) are shown in Figures S1 (shown in Supporting Information) and Figure 1, respectively. The geometries of $C_{60}$ (denoted as *S10*) and its BN substitution compound, $C_{20}(BN)_{20}$ (*10*), were also calculated for the purpose of comparison. The optimized geometric parameters of pure fullerenes are comparable with those previously reported.[26] Their total energies and "BN belt + carbon cap" structures are summarized in Table 1.

**A. Geometries of $C_n$ Fullerenes and Their BN Substitutional Compounds.** As most of the pure $C_n$ structures are being reported for the first time, their geometrical characteristics are discussed briefly for the aim of giving better interpretations of their BCN analogues. The side frames of the pure carbon fullerenes exhibit both the zigzag and armchair nanotube-like structure. According to the tubular construction as well as the polar structure of fullerenes, pure compounds *S1*−*S10* could be classified into three types: (i) Fullerenes containing a zigzag

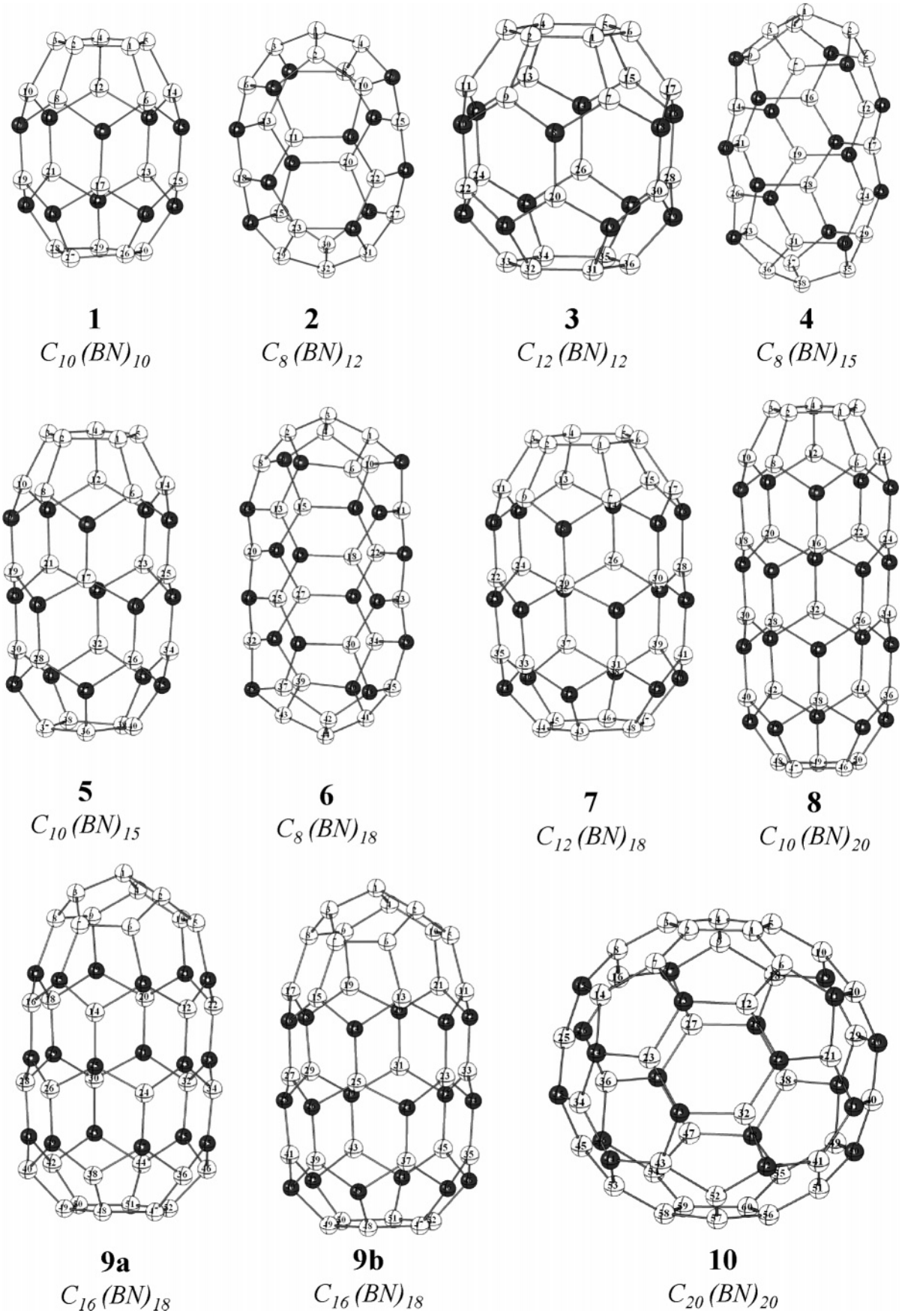


**Figure 1.** 3D diagrams of BCN fullerenes.

(*5, 0*) tubular belt crowned with pentagon caps on each side of the principal axis, including compounds *S1* ($C_{30}$), *S5* ($C_{40}$), and *S8* ($C_{50}$). In these fullerenes the geometries do not adopt perfect symmetry due to the Jahn−Teller effect, i.e., the geometries of $C_{30}$ and $C_{50}$ distort from ideal $D_{5h}$ to $C_{2h}$ symmetry and the symmetry of $C_{40}$ reduces to $C_{2v}$ from $D_{5d}$ symmetry. Our results

**TABLE 1: B3LYP/6-31G(d) Total Energies (Hartree) of Carbon Fullerenes and Substituted BCN Fullerenes as Well as Their Nanotube-like Structures**

| | | | | substituted | | structure | |
|---|---|---|---|---|---|---|---|
| no. | fullerene | $E_{total}$ | | BCN fullerene | $E_{total}$ | BN belt | cap |
| S1 | $C_{30}$ | −1142.4647 | 1 | $C_{10}(BN)_{10}$ | −1177.4978 | zigzag (*5,0*) | pentagon |
| S2 | $C_{32}$ | −1218.7134 | 2 | $C_8(BN)_{12}$ | −1260.6695 | armchair (*3,3*) | trihedron |
| S3 | $C_{36}$ | −1371.2549 | 3 | $C_{12}(BN)_{12}$ | −1413.2687 | zigzag (*6,0*) | hexagon |
| S4 | $C_{38}$ | −1447.2829 | 4 | $C_8(BN)_{15}$ | −1499.6934 | armchair (*3,3*) | trihedron |
| S5 | $C_{40}$ | −1523.4041 | 5 | $C_{10}(BN)_{15}$ | −1576.0133 | zigzag (*5,0*) | pentagon |
| S6 | $C_{44}$ | −1675.8393 | 6 | $C_8(BN)_{18}$ | −1738.8578 | armchair (*3,3*) | trihedron |
| S7 | $C_{48}$ | −1828.4919 | 7 | $C_{12}(BN)_{18}$ | −1891.5504 | zigzag (*6,0*) | hexagon |
| S8 | $C_{50}$ | −1904.3607 | 8 | $C_{10}(BN)_{20}$ | −1974.5389 | zigzag (*5,0*) | pentagon |
| S9 | $C_{52}$ | −1980.8688 | 9a | $C_{16}(BN)_{18}$ | −2043.8727 | zigzag (*6,0*) | hexagon and trihedron |
| | | | 9b | | −2043.8850 | | |
| S10 | $C_{60}$ | −2286.1705 | 10 | $C_{20}(BN)_{20}$ | −2355.9199 | armchair (*5,5*) | pentagon |

show that in these structures the planes of the upmost/downmost pentagons collapse due to one carbon belonging to the pentagon moving inward. Taking $C_{30}$ for example, the torsion angle between the introflexional carbon and other four atoms is 4.7° at the B3LYP/3-21G* level of optimization (Figure 2a). The equivalent dihedral angles in $C_{40}$ and $C_{50}$ are 0.4° and 0.5°, reaching a planar structure overall. Nevertheless, the delocalization of $\pi$ electrons within the polar pentagon atoms in $C_{30}$, $C_{40}$, and $C_{50}$ is weaker than that in the absolute planar structure. In addition, the zigzag (*5*, 0) C-NT-like belts of these fullerenes have a very small diameter of about 4.1 Å. As a result, the parallel conjugate hexagons encircling the equator are significantly strained in which the carbon atoms connected with the polar pentagons move outward with dihedral angles of about 159.3°. $C_{40}$ and $C_{50}$, containing similar but elongated tubular belts, show similar structural characteristics to those of $C_{30}$.

Due to the above-mentioned similarities between BN and carbon, the BN substitutional analogues (*1*, *5*, and *8* in Figure 1) of type i fullerenes do not show a significant structural difference compared to their parent compounds. Besides the known BN substitution effect, i.e., the B atom moves inward while the N atom moves outward, which leads to a larger diameter of about 4.3 Å for BN tubular belts, the main variance in BCN hybrid fullerenes is the flatness of two polar pentagons. As shown in Figure 2b, the flatness of the downmost pentagon at the N side evidently collapses where an atom moves outward with a dihedral angle of about 10.0°; meanwhile, atoms in the other polar pentagon at the B side reach perfect planarity. Similar trends were observed in $C_{10}(BN)_{15}$ and $C_{10}(BN)_{20}$ in which the dihedral angles are 10.2° and 9.8°, respectively. The geometric variations of BCN fullerenes, produced by the anisotropic properties of BN-NTs, lead to different properties compared with their carbon analogues, in particular the molecular electrostatic distributions, which will be discussed in the subsequent section.

(ii) Compounds *S2* ($C_{32}$), *S4* ($C_{38}$), and *S6* ($C_{44}$) represent a new type of structure in which the armchair (*3*, *3*) side frame is ended with three-member trihedral caps. This series of fullerenes ($C_{32}$, $C_{38}$, and $C_{44}$) shows distinct differences with fullerenes of type i and type iii, i.e., their dipolar trihedral caps have the weakest delocalization of $\pi$ electrons. The upmost/downmost carbon atoms in the spindly structures prefer $sp^3$-like hybridization, which leads to vertical lone pair electrons on each side of the 3-fold symmetry axis. On average, the diameter of the tubular belts is 4.3 Å, also indicating a strong strained conjunct structure. Another trend is that the lengths of the latitudinal C−C bonds in armchair frames (in particular the bonds near and away from the equator) are becoming more and more similar along with an increase of the width of the belts from $C_{32}$ to $C_{38}$ and $C_{44}$, which indicates that the fullerenes show more and more character of C-NTs. The BN-substituted results of these fullerenes (*2*, *4*, and *6* in Figure 1) do not show obvious structural alternations except for the known B and N distortions. Because the strain effect of the armchair (*3*, *3*) acts almost evenly on all of its bonds, differing from the strain force concentrating on partial bonds in zigzag (*5*, *0*) and zigzag (*6*, *0*) structures, the diameters of the BN belts increase less than 0.05 Å compared with those in pure fullerenes, consistent with recently reported structural parameters of armchair (*3*, *3*) BN-NTs.[36]

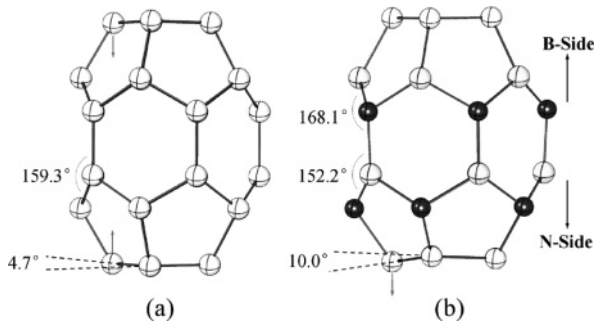


**Figure 2.** B3LYP/3-21G*-optimized geometries of (a) $C_{30}$ and (b) $C_{10}(BN)_{10}$.

(iii) Fullerenes with a zigzag (*6*, *0*) belt joined to hexagonal terminal caps, including compounds *S3* ($C_{36}$), *S7* ($C_{48}$), and *S9* ($C_{52}$) (for compound *9*, a hexagon and a 10-membered trihedron are on each side of the tubular framework). In these compounds $C_{36}$ and $C_{48}$ have perfect $D_{6h}$ and $D_{6d}$ symmetries, respectively. Compared with those in zigzag (*5*, *0*) and armchair (*3*, *3*) side frames, the overstrain effect among parallel pentagons in zigzag (*6*, *0*) comes loose due to the increase of the diameter of the tube (5.0 Å). The polar hexagons are completely planar; thus, strong delocalization of the $\pi$ electrons within them could be expected. In addition, the C−C bonds between the polar hexagons and the zigzag (*6*, *0*) side frames are systematically longer than those in compounds of type i, also indicating the weaker interaction between these two regions.

The BN substitutional analogues (*3*, *7*, and *9* in Figure 1) inherit the high symmetric structures from their parent compounds. In these compounds the diameter of the BN belts increases to 5.1 Å, close to the previously reported value of 5.0 Å for zigzag (*6*, *0*) BN tubes.[36] The carbon hexagonal caps are both planar, differing from those being found in their zigzag (*5*, *0*) counterparts. The exception occurs in the substitutional doping of $C_{52}$. Since the two polar regions of $C_{52}$ are not equivalent, the boron−nitride substitution of $C_{52}$ leads to two compounds, *9a* and *9b* (in Figure 1); in the former the hexagon cap connects to the B side of the tube, while in the latter the hexagon connects to the N side instead.

As important properties to evaluate the stabilities of nanocages, the heats of atomization of pure carbon fullerenes and

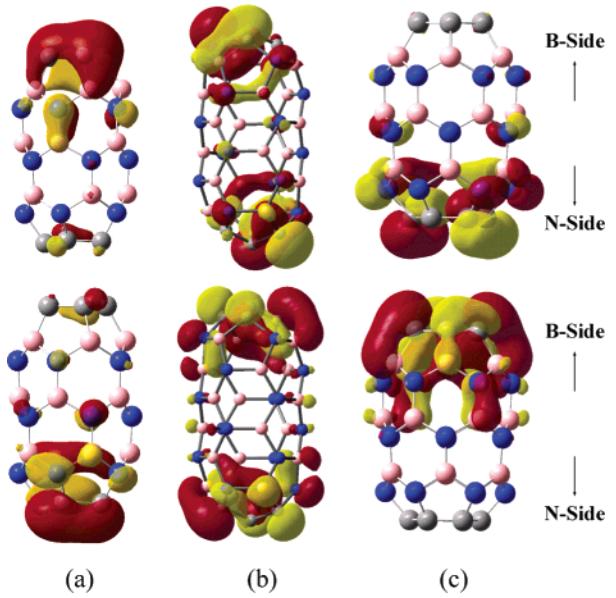


**Figure 3.** Kohn−Sham orbital characters of the HOMOs (top) and LUMOs (bottom) of fullerenes: (a) $C_{10}(BN)_{15}$, (b) $C_8(BN)_{18}$, and (c) $C_{12}(BN)_{18}$ (negative values are in yellow and positive value in red).

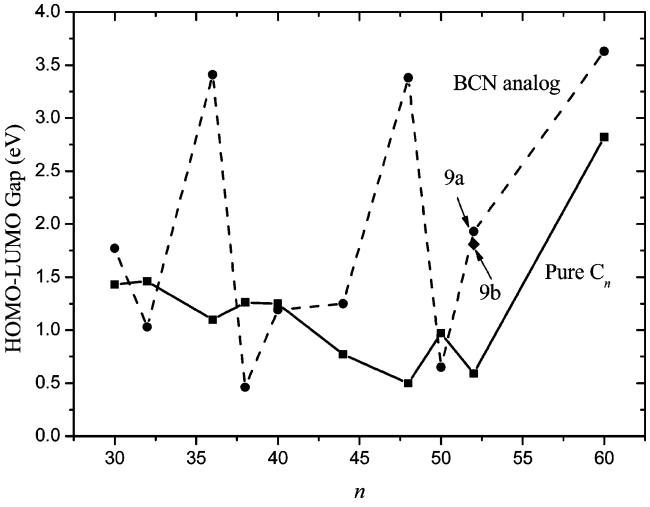


**Figure 4.** Variation of the HOMO−LUMO gaps of pure fullerenes and BN substitutional analogues against the total number of atoms.

their BN-substituted analogues were calculated at the B3LYP/6-31G(d) level. It was found that from $C_{30}$ to $C_{60}$ the heat of atomization values increase from 4440 to 9660 kcal·mol$^{-1}$. As we know, a lower heat of atomization corresponds to higher energy, thus making them less stable and harder to synthesize. As a result, the stability from $C_{30}$ to $C_{60}$ fullerenes increases with the number of carbon atoms. A similar trend was found in the BCN fullerenes, despite of their heat of atomization values being slightly smaller than the corresponding parent compounds. These findings predict that BN-substituted fullerenes have comparable stabilities to pure carbon systems. Variations of the heat of atomization (in kcal·mol$^{-1}$) of pure fullerenes and BN substitutional analogues against the total number of atoms can be found in the Supporting Information (Figure S2).

As a whole, the equatorial substitutional doping of BN does not significantly alter the structure and stabilities of parent carbon fullerenes, except for type i compounds (the ones with a zigzag (*5, 0*) side frame) where larger geometric distortions were observed in polar pentagons. In addition, the diameters of the fullerenes slightly increase during the introduction of BN dopants.

**B. HOMO−LUMO Characters and Energy Gap.** It is useful to examine the energy level and character of the HOMO and LUMO, which are associated with the chemical reactivity, electron excitation, etc. Therefore, the Kohn−Sham HOMO and LUMO characters of nine $C_n$ fullerenes as well as their BN analogues were investigated (all figures are illustrated in the Supporting Information). For those of carbon fullerenes the main characters are laterally symmetric about the equatorial plane (except for $C_{52}$ which has an asymmetric skeleton); no more analyses performed. The electronic cloud distributions in the front orbitals of CBN fullerenes show an interesting distinctness according to their different types of structures defined in section A. The orbital characters of part of the BCN fullerenes are depicted in Figure 3, where $C_{10}(BN)_{15}$, $C_8(BN)_{18}$, and $C_{12}(BN)_{18}$ are selected as being representative of BCN fullerenes from type i to type iii. The HOMO of $C_{10}(BN)_{15}$ (which has a zigzag (*5, 0*) side frame) is localized predominately near the perfect planar pentagon on the B side, whereas its LUMO is from the N side of the fullerene, near the distorted pentagon. This implies a trend of electron transfer from the B side to the N side in type i fullerenes during electronic excitations. On the contrary, the distributions of the HOMOs and LUMOs for type iii fullerenes with zigzag (*6, 0*) side frames are definitely in opposition to those of type i. For instance, the HOMO of $C_{12}(BN)_{18}$ is localized on the polar hexagon at the N side, while its LUMO is contributed from the hexagon from the B side; thus, a reverse electron-transfer direction is expected during electron excitation. For the asymmetric fullerene $C_{52}$, BN substitution leads to two compounds *9a* and *9b* (Figure 1). Both the HOMO and LUMO of *9a* are predominantly localized on the 10-membered trihedral caps at the N side; for *9b*, the distribution of the LUMO shows a similar trend with *9a* while the HOMO concentrates near the hexagon. In addition, front orbital distributions of type ii compounds are localized on either side of fullerenes, separated by the armchair (*3, 3*) side frame. Therefore, intramolecular electron transfers of this series of compounds are unexpected for the balance of the HOMO and LUMO distributions. In conclusion, equatorial BN substitutional doping will definitely alter the HOMO and LUMO characters of the fullerenes, and the orbital distributions of BCN hybrid fullerenes depend on the indexes of BN tubular belts, differing from zigzag (*5, 0*) to zigzag (*6, 0*) and armchair (*3, 3*).

Besides the characters of the HOMO and LUMO, energy gaps are of importance for nanotubes and fullerenes as electronic devices due to their direct association with the band gap of the solid;[19] in addition, they also are closely related to the chemical stability against electron excitation with larger gaps corresponding to greater stabilities. As shown in Figure 4, in general, the HOMO−LUMO gaps of $C_n$ fullerenes become narrower with the increasing number of carbon atoms, except for $C_{60}$, which has the largest band gap as well as the greatest thermodynamic and kinetics stabilities among the studied fullerenes. The HOMO−LUMO gaps of BCN fullerenes are somehow complicated; thus, it is difficult to say that BN doping will increase or decrease the energy gaps of fullerenes. This was also shown to be true by Kar et al. for mono-BN-substituted small fullerenes.[26] Some conservative conclusions could be drawn: the band gaps of type i and type ii compounds do not change significantly during BN doping, whereas the BN substitutional doping of type iii compounds significantly increases the band gaps, suggesting greater stabilities against electron excitation. It also needs to be mentioned that band gaps calculated in the current investigation might not be comparable with those of

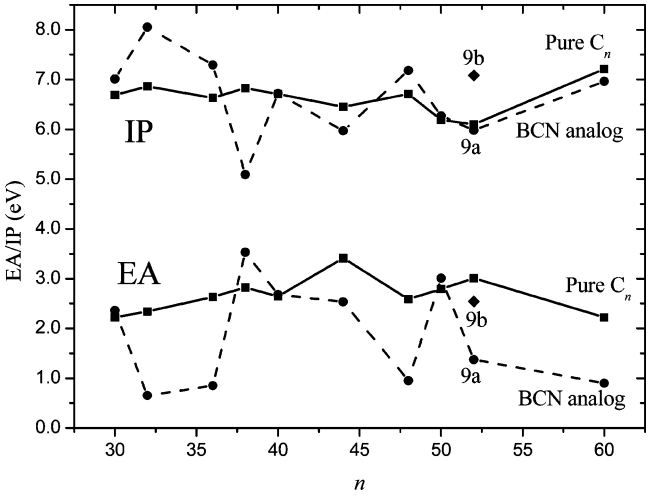


**Figure 5.** Variation of the electron affinities (EA) and ionization potential (IP) of pure fullerenes and BN substitutional analogues with the total number of atoms.

previously reported ones because the $C_n$ isomers selected here may not be the most energy-favorable ones of fullerenes.

**C. Electron Affinities and Ionization Potentials.** The effects of BN substitution on the IP and EA of fullerenes have been investigated by several groups;[23−27] conclusions differ from one group to the other depending on the system studied. For $C_{50}$ BN doping decreases the EA and increases the IP,[27] while for $C_{60}$ the author declared substituted fullerenes have a smaller ionization potential relative to pure fullerenes and thus heterofullerenes are good electron donors.[26] Both conclusions are based on very thorough studies and are therefore reliable. The electron affinities and ionization potentials of the pure and doped fullerenes are compared in the lower and upper portions of Figure 5, respectively. From Figure 5, no systematic trends were found in the variation of both EA and IP. For the electron affinities, the BN doping of type i fullerenes leads to similar EA values compared with their parent compounds, which means that substitution does not change the reduction properties. For type ii and type iii fullerenes, a rough trend was found where the decrease of the EA values during BN doping implies easier reduction tendencies; the only exception occurs in the doping of $C_{38}$, with a somewhat increase of EA. The variations of the IP are systematically smaller than what occurs in EA; in addition, no obvious trends with regard to the effects of substitution were observed. This reflects that BN doping might exerts less of an influence on the oxidation properties than the reduction properties.

**D. MEP Distributions and Aromaticities.** In a very recent study Jemmis et al. suggested the molecular electrostatic potential to be a powerful tool for the analysis of a variety of chemical phenomena, in particular, the local $\pi$-electron concentrations explaining the aromatic character.[37] Even though many studies have been reported on the MEP of aromatic systems, few studies are available for fullerenes and are rare for their corresponding BCN hybrid systems. Therefore, the MEP characters of carbon fullerenes were investigated in the first instance. The ESP isosurfaces for $C_{30}$, $C_{32}$, and $C_{36}$, which represent BCN hybrid systems of type i, type ii, and type iii respectively, are shown in Figure 6 (more figures are given in Figure S3, Supporting Information). On the whole, the electrostatic distribution in carbon fullerenes is symmetric through the diametral plane: the tubular framework is encircled with a positive-valued MEP isosurface, while both the upmost/downmost polar regions are covered with a negative potential from

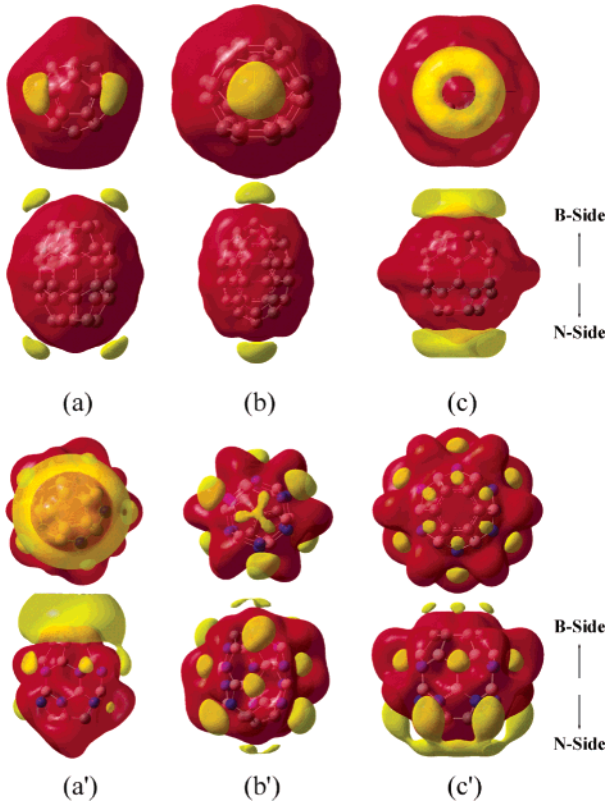


**Figure 6.** MEP isosurface for (a) $C_{30}$, (b) $C_{32}$, and (c) $C_{36}$ and their BCN analogues (a′) $C_{10}(BN)_{10}$, (b′) $C_8(BN)_{12}$, and (c′) $C_{12}(BN)_{12}$. The top views are shown in the first row and side views at the bottom; the contour values are 0.0075 au except for a′ with 0.015 au.

either the strong delocalization of $\pi$ electrons within the pentagon/hexagon (for type i and iii) or a lone-pair electron from a $sp^3$-like hybridized orbital of the trihedral carbon (for type ii). This indicates in these fullerenes, in particular those of type i and type iii, that aromaticities within polar pentagonal/hexagonal rings are significantly stronger than those among side frameworks. These results are in good agreement with our previous work about $C_{20}$ and $C_{60}$.[38]

The MEP distributions of BN fullerenes distinctly differ from their carbon counterparts, especially in the negative-valued region. Though the negative MEP is also located predominantly over the polar regions, the symmetries through the diametral plane are no more prominent in type i and type iii compounds (seen in Figure 6, a′−c′) due to the anisotropic effect of zigzag BN tube. In these two types of fullerenes the negative MEP distributions depend on the planarity of the polar C rings as well as the stretching direction of the BN tube. For instance, the negative MEP of $C_{10}(BN)_{10}$ (type i) localizes over the B-side pentagon, which has better flatness than the other one, though stronger electronic concentrations are expected in the other pentagon at the N side due to the electron contribution from nitrogen atoms; meanwhile, the negative-valued region of $C_{12}(BN)_{12}$ (type iii) covers the N-side hexagon, which has a stronger electron concentration due to the electron-donating effects of adjacent nitrogen atoms than the other side. This is still validated in asymmetric compound *9b* (Figure 1), while in case of *9a* the negative MEP locates over the 10-membered trihedral caps at the N side. The negative MEP distribution of type ii compound $C_8(BN)_{12}$ is spread all over the fullerenes, coming from lone-pair electrons of $sp^3$ carbon in polar caps and nitrogen atoms from the side tube. In addition, the previous work of Moon et al.[39] revealed that the nitrogen atoms in BN-NTs are partially $sp^3$ hybridized. The electrostatic distribu-

tions of our study also support this point of view, since localized negative-valued MEP concentrations were found over the nitrogen of BN belts. In conclusion, the MEP distribution of hybrid BN fullerenes differs from one type to another, depending on the indexes of their BN belts.

## Conclusions

The full equatorial hexagonal substituted BCN fullerenes were first characterized based upon density functional theory in comparison with their parent fullerenes $C_n$ ($n$ = 30, 32, 36, 38, 40, 44, 48, 50, 52). The substitutional structures, HOMO−LUMO energy gaps, ionization potentials, electron affinities, as well as molecular electrostatic potentials of the BCN hybrid fullerenes have been investigated extensively. From the results obtained in the present investigation we emphasize the following important points.

The BN-substituted fullerenes studied comprised of a tubular "belt" and polar "cap" could be considered as being intermediate between fullerenes and BN-NTs. According to the tubular construction as well as the polar structure, fullerenes could be divided into three types: type i containing a zigzag (*5, 0*) tubular belt crowned with pentagon caps on each side; type ii in which the armchair (*3, 3*) side frame is ended with three-membered trihedral caps; and type iii constructed from a zigzag (*6, 0*) belt joined to hexagonal terminal caps. The BN substitutional effects significantly depend on the types of fullerenes.

The dependencies between properties of BCN hybrid fullerenes and the type of "tubular belt + polar cap" structures are tested to be valid in the HOMO−LUMO energy gaps, ionization potentials, electron affinities, as well as molecular electrostatic potentials. Especially, the HOMO and LUMO characters and MEPs of BCN fullerene are strongly governed by the above-mentioned types of structures. It is hard to simply summarize straightforward tendencies of their properties in the absence of structural characters. The results of this work might lead to nanoparticles with unusual electronic properties as promising candidates for electronic devices.

**Acknowledgment.** This project was supported by the National Natural Science Foundation of China (Contract Nos. 20573032, 20503035) and Nature Science Foundation of Hebei Province (Contract Nos. B2004000147, B20006000137).

**Supporting Information Available:** Optimized structures, orbital characters of the HOMOs and LUMOs, as well the ESP isosurface of $C_n$ fullerenes and their BCN counterparts (pdf). This material is available free of charge via the Internet at http://pubs.acs.org.

## References and Notes

(1) Kroto, H. W.; Health, J. R.; O'Brien, S. C.; Curl, R. F.; Smalley, R. E. *Nature* **1985**, *318*, 162.
(2) Iijima, S. *Nature* **1991**, *354*, 56.
(3) Ebbesen, T. W.; Ajayan, P. M. *Nature* **1992**, *358*, 220.
(4) Ebbesen, T. W.; Hiura, H.; Fujita, J.; Ochiai, Y.; Matsui, S.; Tanigaki, K. *Chem. Phys. Lett.* **1993**, *209*, 83.
(5) Iijima, S. *Mater. Sci. Eng. B* **1993**, *19*, 172.
(6) Sattler, K. *Carbon* **1995**, *33*, 915.
(7) Liang, W.-Z.; Yokojima, S.; Ng, M.-F.; Chen, G.-H.; He, G.-Z. *J. Am. Chem. Soc.* **2001**, *123*, 9830.
(8) Prinzbach, H.; Weiler, A.; Landenberger, P.; Wahl, E.; Worth, J.; Scott, L.; Gelmont, M.; Olevano, D.; Issendorff, Bv. *Nature* **2000**, *407*, 60.
(9) Kietzmann, H.; Rochow, R.; Ganteför, G.; Eberhardt, W.; Vietze, K.; Seifert, G.; Fowler, P. W. *Phys. Rev. Lett.* **1998**, *81*, 5378 and references therein.
(10) Voytekhovsky, Y. L.; Stepenshchikov, D. G. *Acta Crystallogr., Sect. A: Found. Crystallogr.* **2001**, *A57*, 736.
(11) Raghavachari, K.; Strout, D. L.; Odom, G. K.; Scuseria, G. E.; Pople, J. A.; Johnson, B. G.; Gill, P. M. W. *Chem. Phys. Lett.* **1993**, *214*, 357.
(12) Saito, M.; Miyamoto, Y.; Okada, S. *Mol. Cryst. Liquid Cryst.* **2002**, *386*, 97.
(13) Menon, M.; Srivastava, D. *J. Mater. Res.* **1998**, *3*, 2357.
(14) Kietzmann, H.; Rochow, R.; Ganteför, G.; Eberhardt, W.; Vietze, K.; Seifert, G.; Fowler, P. W. *Phys. Rev. Lett.* **1998**, *81*, 5378 and references therein.
(15) Prinzbach, H.; Weller, A.; Landenberger, P.; Wahl, F.; Wörth, J.; Scott, L. T.; Gelmont, M.; Olevano, D.; Issendorff, B. V. *Nature* **2000**, *407*, 60.
(16) Lu, X.; Chen, Z.-F. *Chem. Rev.* **2005**, *105*, 3643.
(17) Dresselhaus, M. S.; Dresselhaus, G.; Eklund, P. C. *Science of Fullerenes and Carbon Nanotubes*; Academic Press: New York, 1996.
(18) Xie, R.-H.; Bryant, G. W.; Zhao, J.; Smith, V. H., Jr.; Carlo Di A.; Pecchia, A. *Phys. Rev. Lett.* **2003**, *90*, 206602.
(19) Xie, R.-H.; Bryant, G. W.; Sun, G.-Y.; Kar, T.; Chen, Z.-F.; Smith, V. H., Jr.; Araki, Y.; Tagmatarchis, N.; Shinohara, H.; Ito, O. *Phys. Rev. B* **2004**, *69*, 201403(R).
(20) de Heer, W. A.; Bacsa, W. S.; Châtelain, A.; Gerfin, T.; Humphrey-Baker, R.; Forro, L.; Ugarte, D. *Science* **1995**, *268*, 845.
(21) Blase, X.; Rubio, A.; Louie, S. G.; Cohen, M. L. *Europhys. Lett.* **1994**, *28*, 335.
(22) Cumings, J.; Zettl, A. *Chem. Phys. Lett.* **2000**, *316*, 211.
(23) Pattanayak, J.; Kar, T.; Scheiner, S. *J. Phys. Chem. A* **2001**, *105*, 8376.
(24) Pattanayak, J.; Kar, T.; Scheiner, S. *J. Phys. Chem. A* **2002**, *106*, 2970.
(25) Kar, T.; Pattanayak, J.; Scheiner, S. *J. Phys. Chem. A* **2003**, *107*, 8630.
(26) Pattanayak, J.; Kar, T.; Scheiner, S. *J. Phys. Chem. A* **2003**, *107*, 4056; *J. Phys. Chem. A* **2004**, *108*, 7681 and references therein.
(27) Xu. X.-F.; Shang, Z.-F.; Wang, G.-C.; Li, R.-F.; Cai, Z.-S.; Zhao, X.-Z. *J. Phys. Chem. A* **2005**, *109*, 3754 and references therein.
(28) Ajayan, P. M.; Iijima, S. *Nature* **1992**, *358*, 23.
(29) Sun, L.-F.; Xie, S.-S.; Liu,-W.; Zhou, W.-Y.; Liu, Z.-Q.; Tang, D.-S.; Wang, G.; Qian, L.-X. *Nature* **2000**, *403*, 384.
(30) Peng, H.-Y.; Wang, N.; Zheng, Y.-F.; Lifshitz, Y.; Kulik, J.; Zhang, R.-Q.; Lee, C.-S.; Lee, S.-T. *Appl. Phys. Lett.* **2000**, *77*, 2831.
(31) Fullerene structure library presented by Mitsuho Yoshida via the Internet at http://www.cochem2.tutkie.tut.ac.jp/Fuller/Fuller.html.
(32) Becke, A. D. *J. Chem. Phys.* **1992**, *96*, 2155.
(33) Becke, A. D. *J. Chem. Phys.* **1993**, *98*, 5648.
(34) Gadre, S. R.; Shirsat, R. N. *Electrostatics of Atoms and Molecules*; Universities Press: Hyderabad, India, 2000.
(35) Frisch, M. J.; Trucks, H. B.; Schlegel, G. W.; Scuseria, G. E.; Robb, M. A.; Cheeseman, J. R.; Zakrzewski, V. G.; Montgomery, J. J. A.; Stratmann, R. E.; Burant, J. C.; Dapprich, S.; Millam, J. M.; Daniels, A. D.; Kudin, K. N.; Strain, M. C.; Farkas, O.; Tomasi, J.; Barone, V.; Cossi, M.; Cammi, R.; Mennucci, B.; Pomelli, C.; Adamo, C.; Clifford, S.; Ochterski, J.; Petersson, G. A.; Ayala, P. Y.; Cui, Q.; Morokuma, K.; Malick, D. K.; Rabuck, A. D.; Raghavachari, K.; Foresman, J. B.; Cioslowski, J.; Ortiz, J. V.; Baboul, A. G.; Stefanov, B. B.; Liu, G.; Liashenko, A.; Piskorz, P.; Komaromi, I.; Gomperts, R.; Martin, R. L.; Fox, D. J.; Keith, T.; Al-Laham, M. A.; Peng, C. Y.; Nanayakkara, A.; Gonzalez, C.; Challacombe, M.; Gill, P. M. W.; Johnson, B.; Chen, W.; Wong, M. W.; Andres, J. L.; Gonzalez, C.; Head-Gordon, M.; Replogle, E. S.; Pople, J. A. *Gaussian 98*; Gaussian, Inc.: Pittsburgh, PA, 1998.
(36) Xu, H.; Ma, J.; Chen, X.; Hu, Z.; Huo, L.-F.; Chen, Y. *J. Phys. Chem. B* **2004**, *108*, 4024.
(37) Phukan, A. K.; Kalagi, R. P.; Gadre, S. R.; Jemmis, E. D. *Inorg. Chem.* **2004**, *43*, 5824.
(38) Liu, F.-Y.; Meng, L.-P.; Zheng, S.-J. *J. Mol. Struct. (THEOCHEM)* **2005**, *725*, 71.
(39) Moon, W. A.; Hwang, H. J. *Physica E* **2004**, *23*, 26.